Journal of Power Sources, 6 (1981) 101 - 120

THE ELECTROCHEMISTRY OF THE POROUS LEAD ELECTRODE IN SULPHURIC ACID — A SELECTIVE REVIEW

N. A. HAMPSON and J. B. LAKEMAN*

Department of Chemistry, University of Technology, Loughborough, Leics. LE11 3TU (Gt. Britain)

(Received April 26, 1980)

Summary

The electrochemistry of the porous lead electrode, both theory and practice, is reviewed and the influence of additives on the performance and behaviour of the electrode is discussed. Important aspects such as life under different cycling regimes and low temperature performance are also examined.

The review contains 149 references.

Introduction

In 1971, Burbank *et al.* [1] reviewed some aspects of research into the electrochemistry of the lead–acid battery. In 1977, Ruetschi [2] discussed the history, development, and science of the system, and this was followed in 1979 [3] by a critical analysis of the future rôle of the cell in the context of other systems under development. An account of the technological aspects of the battery was published in 1977 [4], which complemented Vinal's classic, *Storage Batteries* [5].

In the lead–acid battery, electrical energy is produced from the reaction:

$$Pb + PbO_2 + 2H_2SO_4 \rightarrow 2PbSO_4 + 2H_2O \quad (1)$$

The reaction occurs at porous, active masses supported on lead alloy grids; the grids act as current collectors and the cell contains sulphuric acid in excess of the requirements of reaction (1). The positive and negative electrodes are normally separated by microporous sheets which prevent short-circuiting, and shedding of active material from the electrodes.

*Present address: Chloride Alcad Ltd., Redditch, Worcs., England.

The equation for the negative electrode may be written as

$$Pb + SO_4^{2-} \underset{\text{charge}}{\overset{\text{Discharge}}{\rightleftharpoons}} PbSO_4 + 2e. \quad (2)$$

The charge/discharge cycle at the negative electrode involves a considerable redistribution of the active material during the dissolution, nucleation, and growth of the solid phases. In the electrolyte, uncharged species can be transported by diffusion and convection, whereas ions can also move by migration in an electric field. The occurrence of one or all of these modes of transport depends on electrode properties such as geometry, porosity, conductivities of the solid and liquid phases, and the current/voltage characteristics of the electron transfer reaction. Modelling of the negative electrode is further complicated owing to the change in electrode volume that occurs on cycling; the lower density of $PbSO_4$ effects a decrease of cell porosity on discharge.

Because of the highly complex behaviour of the negative electrode, attempts to improve battery performance have taken a rather empirical approach, which has proved costly and time-consuming. With so many factors interacting to determine the overall electrode behaviour, a highly detailed knowledge of the electrode is required to achieve an optimum combination of all the possible variables. Steps have been taken to achieve this through the development of theories explaining the behaviour of porous electrodes.

1. Porous electrode theory

Industrial electrodes are normally porous because it is necessary to carry out electrode reactions at significantly high current densities. The specific surface area of porous lead electrodes has been determined as ~ 0.3 - 0.46 $m^2\ g^{-1}$ [6, 7], although the effective surface area is quoted as ~ 0.04 - 0.05 $m^2\ g^{-1}$ [8, 9]. Because of the large surface area of the porous electrode, the driving force for the reaction, the overvoltage, is smaller. However, the current distribution in the practical porous electrode is non-uniform because of the mass-transfer and ohmic hindrances. The capacity/performance of the porous lead electrode is determined by the following factors [10]:

(a) the amount of active material in the electrode;
(b) the thickness of the electrode;
(c) the rate of discharge;
(d) the temperature;
(e) the quantity and concentration of the electrolyte;
(f) the porosity;
(g) the design of the electrode;
(h) the previous history of the electrode.

The task of modelling the electrode to account realistically for all these factors is daunting, and porous electrode theory has to be developed in con-

cert with experimental observations. The porous electrode model is, at best, a simplified mathematical expression for the transport and kinetic phenomena occurring at the electrode. Various assumptions have to be made, and each one involves its own limitations. The goal of porous electrode modelling is the provision of design criteria for the perfectly optimised electrode. The model has to be based on analyses of actual elementary processes occurring within the electrode matrix, such as transport and charge transfer kinetics. Theoretical aspects of electrode modelling have evolved considerably, from the simple picture of Daniel'-Bek [11], using invariant reaction kinetics and fixed geometry, to the comprehensive models of today.

Work on mathematical modelling has been well reviewed by a number of authors [12 - 15]. The majority of models use a one-dimensional representation, where the pore geometry is ignored. This approach is valid when the distances over which there is significant variation in concentration and potential are large compared with the characteristic dimensions of the pore system. The models of flooded porous electrodes may be divided into three categories [10]: (a) The pore model: represented by parallel cylindrical pores of constant radius, perpendicular to the outer surface [16]. (b) The analogue model: makes use of equivalent circuits, with the resistance of carrier materials and electrolytes in conjunction with polarisation resistance [17, 18]. (c) The macrohomogeneous model: views the electrode on a macroscopic scale and disregards the geometric detail of its structure. The whole electrode–electrolyte system is described as the superposition of two continua: the electrode matrix, and the electrolyte which fills the voids within the matrix. Variables in the two phases, such as potential and current, are regarded as continuous functions of time and space [19]. There are certain drawbacks to models (a) and (b). The pore model is difficult to apply to electrodes which must be considered as two-dimensional, because questions would arise concerning the direction of the pores. In the case of the analogue model, non-linear resistances must be used when the overvoltage does not vary linearly with the current density, and the influence of diffusion cannot be satisfactorily modelled.

These difficulties are eliminated in the case of the macrohomogeneous model, where variables such as matrix and electrolyte conductivities, physical structure and electrolyte conductivity, can be averaged into continuously varying functions in time and space. The model is, therefore, based on equations describing mass transfer, ionic and electronic currents, electrode kinetics, conservation equations for each dissolved species, and, more recently, structural changes of the electrode occurring during cycling. However, the pore model uses equations which are essentially identical [12], yielding complementary results in some cases, and will be discussed in more detail.

(i) The pore model

Work on the pore model up to 1966 has been well reviewed by de Levie [12] and it is sufficient here to report some of the conclusions. The porous electrode is considered as a single pore of uniform cross-section,

homogeneously filled with electrolyte, with a negligible matrix resistance. The curvature of the pore is considered unimportant, and the pore is represented by an RC transmission line. Assuming mass transport is not rate-limiting, but the electrode is reaction-controlled, then the pore behaves like a resistance where

$$\frac{\eta}{i} = (ZZ')^{1/2} \operatorname{cotanh} p'l \tag{3}$$

hence, the current in the porous electrode is inversely proportional to $(ZZ')^{1/2}$, and $p' = (Z/Z')^{1/2}$. In contrast, the current at a flat electrode is inversely proportional to Z'; experimental verification of these predictions will be reported in Section 4.

Austin [20] also considered the case where the porous electrode might be controlled by solution resistance and/or diffusion. Considering a redox system with soluble reactants at inert electrodes, a dimensionless quantity was derived

$$\phi = \frac{\alpha n^2 F^2 CD}{\kappa RT} . \tag{4}$$

Austin [20] concluded that if $\phi > 5$, electrode processes are resistance-controlled; if $\phi < 0.5$, electrode processes are diffusion-controlled. Using eqn. (4) Bode [4] calculated a value of $\phi = 0.7$ for a charged lead–acid battery. This value decreases with discharge and indicates that the performance of the lead–acid battery may be influenced by the diffusion of acid in the porous matrix; this result will be discussed in Section 4.

Another important concept to arise from porous electrode theory is the penetration depth, $1/p'$, which characterises the distance to which a reaction can penetrate a porous electrode [16, 21] (see eqn. (1)). This length indicates the optimum thickness for a porous electrode and has, therefore, considerable significance, because electrodes much thinner than the penetration depth behave like planar electrodes of enhanced surface, while electrodes much thicker than the penetration depth are inefficient. If electrodes could be manufactured at a thickness corresponding to a calculated penetration depth, a battery of improved efficiency could be achieved; this has considerable importance for the lead–acid battery where weight is such an important criterion. Unfortunately, as de Levie [12] has shown, this characteristic length varies with the mechanism of current control. For a reaction-controlled porous electrode [21]

$$1/p' = \left[\frac{RTr\kappa}{2nFi_0}\right]^{1/2} \tag{5}$$

and for diffusion control, Bode [4] has derived

$$1/p' = \frac{CDnF}{i(1-\theta)} . \tag{6}$$

From eqn. (5), Bode [4] calculated a value for the penetration depth of 1 mm for the lead–acid battery. From eqn. (6), the penetration depth varies with reactant concentration, and, hence, the rate of discharge. For low discharge rates, the penetration depth was 3 - 5 mm, and for high discharge rates was 0.12 mm. These values indicate the undesirability of high rate discharges of the lead–acid battery in diffusion-limiting situations, but are only applicable to steady-state regimes.

The measurement of the double-layer capacity of the porous electrode has considerable significance because it directly reflects the amount of surface area available for electrochemical reaction, and is, therefore, a valuable non-destructive method of electrode characterisation. Ksenzhek and Stender [22, 23] were the first to consider the time-dependent response of a porous electrode to a current-step function. For a practical porous electrode, however, de Levie [12] has shown that constant-current conditions cannot be achieved because of the variations in pore size of the electrode. A potential-step technique is more readily applicable, and for a potential-step of amplitude E, the charging current is [24, 25],

$$i = E(C'/\pi Zt)^{1/2} . \tag{7}$$

Therefore, the double-layer charging response of a porous electrode to a potential-step is a current–time transient which decays as $1/\sqrt{t}$. By contrast, for a planar electrode, the current decays linearly with time.

Because the pore model is more restrictive than the macrohomogeneous model, analytical solutions can be found to non-steady-state situations. Even so, compared with the theoretical investigations of the steady state, information on the transient response of flooded porous electrodes is scarce. Early contributions were made by Ksenzhek [26 - 28], Guruvich and Bagotskii [29, 30] and Grens and Tobias [31], and, more latterly, by Rangarajan [32] and Kunimatsu [33]. Winsel [16] looked at transient response under constant-potential and constant-current conditions to model the discharge conditions in storage batteries. Dunning and Bennion [34] used a more sophisticated approach to examine the effects of varying solution properties on the discharge of porous electrodes with sparingly soluble reactants; this is analogous to the porous lead electrode, where $PbSO_4$ is the sparingly soluble reactant. These authors used a single pore model and a pseudo steady-state approach to examine the effect of varying solution conditions on the mass transfer between salt crystallites and the metal surface, and found pore blockage to be a significant cause of capacity limitation. Szpak *et al.* [35] also used the pore model to predict reaction profiles for the charging of porous silver electrodes in 1N KCl, and compared the theoretical results with experimental observations on an idealised porous electrode. This work may or may not be relevant to the porous Pb electrode, as the model assumed a solution–diffusion step for the Ag/AgCl system, which approach for this system is valid, but for the porous Pb electrode this is still a controversial issue.

Winsel *et al.* [36] developed a simple pore model of the positive and negative electrodes to investigate the behaviour of the electrodes at high rate, low temperature discharges. Based on the solution/precipitation model of Vetter [37], and assuming that pore plugging was the capacity limiting process, then the capacity of the negative electrode was found to be proportional to the square of the surface area. At -18 °C, and low electrolyte concentration, calculations showed that pore plugging could be due to the formation of ice crystals as well as to $PbSO_4$.

Because of the geometric complexity of practical industrial porous electrodes, the results obtained with the pore model are treated with some caution. However, it is impossible to consider quantitatively the behaviour of the porous lead electrode unless a model with a high degree of uniformity is used to simplify the mathematics defining overall performance parameters, such as mass transfer, and potential and current distributions. The work of Newman and Tobias [19] showed that using the macrohomogeneous approach, the need for detailed uniformity of the porous matrix was dispensed with, whilst still retaining a realistic representation of the porous electrode.

(ii) The macrohomogeneous model

At a given time, there will be a large range of reaction rates within the pores, the distribution of which will be determined by physical structure, conductivities of electrode and electrolyte, and by parameters that characterise the rate of reaction. This rate distribution directly influences the net power available from a battery and changes during the course of charge or discharge. These microscopic variations are averaged, over the dimensions of the porous electrode, into continuously varying functions. The parallel plate configuration, together with the high conductivity current collectors in most batteries, means that the electrode can be considered uniform over its face. This means that quantities such as potentials, current densities, and concentrations vary only with depth into the electrode, and the problem becomes one-dimensional. These variables can be inter-related by several equations to describe the behaviour of the porous electrode. The structural changes occurring during discharge of porous electrodes (such as the lead electrode) need to be considered. One of the first contributions in this field was made by Alkire *et al.* [38], who investigated flooded porous metal electrodes undergoing structural change by anodic dissolution. Alkire and Place [39] later used the steady-state approach again to examine the transient behaviour of porous electrodes during depletion of a limited quantity of solid reactant.

One of the most comprehensive models has been described by Bennion and coworkers [40, 41] for porous electrodes with sparingly soluble reactants (as in the porous lead electrode). The model is based on the solution of a set of coupled partial differential equations representing the various applicable laws of transport and conservation. The authors allowed for non-uniform current distributions, and also for significant changes in the relative

distribution of reactants and products, but not for the effect of pore-plugging. This model was further refined in 1976 [42] to model specifically the Ag/AgCl electrode, and included allowances for electrode tortuosity. Gidaspow and Baker [43] characterised the structural changes that occur during discharge or charge of storage batteries and emphasised the significance of pore-plugging in capacity limitation.

Specific applications of the macrohomogeneous model to the lead–acid cell have been made by Micka and Rousar [44 - 46], Simonsson [10, 47 - 50], and others [51 - 54], using the steady-state approach to predict current distributions, discharge profiles, and acid depletion profiles.

Micka and Rousar followed the earlier work of Stein [54, 55] in assuming reversible electrode kinetics but included allowances for the effects of volume changes on the porosity of the electrode. These authors examined the positive plate [45], the negative plate [44], and the complete lead–acid cell [46]. For the positive plate, they obtained 22 ordinary differential equations, which were solved using a digital computer. Diffusion coefficients, activity coefficients, and equilibrium potentials were allowed to vary with concentration, but the effect of activation polarisation was ignored. It was found that capacity limitation of the positive plate was largely due to acid depletion at the pore mouth [45]. Modelling of the negative electrode was carried out in an identical manner [44], but in the later paper on the modelling of the whole cell [46], the effect of activation polarisation was considered. It was concluded that the theoretical capacity of the cell is normally limited by the positive plate, and that a certain optimum plate distance exists which gives maximum cell capacity. However, Micka and Rousar [46] neglected the effect of electrolyte concentration gradients between the plates, assuming efficient mixing by convection. Turner [53] considered this unlikely in view of the presence of separators between the plates, and investigated the effects of inter-plate concentration gradients. It was shown that inefficient mass transport limited the capacity of the cell at high discharge rates, and optimisation of plate areas and porosities could lead to an improvement in performance.

The comprehensive work of Simonsson [47 - 50] concentrated on the discharge behaviour of the positive plate, and has been well summarised by the author [10]. It was concluded that the capacity of the positive electrode is mainly determined by the combined effects of structural and mass transfer hindrances; this was confirmed by electron microprobe analysis of $PbSO_4$ in the positive plate [50]. The confirmation of theoretical predictions by direct observations has developed into a necessary and fruitful area of research into porous electrode theory. This aspect deserves separate consideration from indirect observations on the porous lead electrode.

(iii) Experimental verification of porous electrode theory

Experimental verification of the predicted current and potential distributions in the porous electrode has progressed along two paths: those dealing with idealised single pores [56 - 60] and those treating idealised porous

electrodes [35, 38, 61 - 67]. In single pore studies the pore is considered to represent a real electrode made up of multiple aggregates of this pore. However, this technique is rather unrealistic because practical porous electrodes often have smaller pores than can be made artificially, and in real porous electrodes, the pores are interconnected and tortuous. Model electrodes having some resemblance to real electrodes have been studied with varying degrees of success in understanding the prevailing reaction modes and distributions. Generally, electrodes are sectioned after charging or discharging and the current distribution inferred from chemical changes. Electron microprobe analysis has proved particularly useful [47], but surface morphology investigations have also been used [63, 64].

Experimental verification of the modelling of porous electrodes using model or real electrodes, as opposed to single pores, is obviously more relevant to the industrial situation. The experimental studies or the developed mathematical representations can be used separately, but together they provide the most valuable means for optimising electrode performance. Experimental verification of porous electrode theory using the positive and negative plates of the lead–acid cell has tended to use standard industrial electrodes which were analysed for $PbSO_4$ after discharging to different levels at varying rates.

Formerly, this analysis was carried out by the autoradiographic technique using ^{35}S-labelled H_2SO_4 [68 - 73], but this has been superseded by the improved resolution of the electron microprobe analyser [47, 74 - 76]. Yantschenko and Selitsky [77] used a sectioned electrode and measured the current in each section; this technique has been used for other electrodes [61, 62], but it again suffers from poor resolution. Simonsson and his coworkers [50] used conductivity measurements to investigate the effect of structural changes on the conductivity of the pore electrolyte and found extensive pore plugging of the positive electrode at low discharge rates. These authors reproduced the classical forced-flow experiments of Liebnow [78] to demonstrate that the high rate discharge capacity of the positive electrode suffered from mass transfer limitations; similar results were reported by Haebler *et al.* [76].

Studies on the porous electrodes of the lead–acid battery generally confirm the predictions of mathematical modelling; at high discharge rates, the reaction is largely confined to the front of the electrode, but at low discharge rates there is a more even distribution of the product $PbSO_4$. Major difficulties arise in attempting to transform the theoretically derived optimisations into real electrodes because of the intransigence of the present methods of electrode manufacture.

Winsel [78a] has shown that for the lead electrode the pore model and the macrohomogeneous model are completely equivalent. Whilst the Winsel pore model has the advantage that it uses only measurable quantities, it is difficult to construct properly in terms of the actual morphology of a porous lead surface and at present it is not as useful as the macrohomogeneous model. The pore model is, however, to be preferred if it can be set up.

2. The manufacture of the porous lead electrode

The lead electrode most commonly associated with the lead–acid battery is the pasted plate configuration introduced by Fauré in 1881 [79]. This is manufactured by applying a paste, made of incompletely oxidised lead powder and sulphuric acid, to a cast lead-alloy grid structure. The electrode is then "cured", followed by reducing (charging) in dilute sulphuric acid, to form sponge lead. The manufacture of the porous lead electrode has been comprehensively treated [4, 5] and the materials and mechanisms of the lead–acid battery have been recently reviewed [80]. It is sufficient here to review briefly the pasting, curing, and forming processes.

(i) Pasting

The grid which forms the basis of the porous lead electrode acts as a current collector to the active material, which is also held in place by the mesh of the grids. Numerous grid geometries have been used [5] and alloying additions are made to improve the functioning of the grid, which has to withstand electrochemical corrosion and act as a load-bearer for the active material. Grids are normally cast, and to achieve optimal castability, corrosion performance, and load-bearing characteristics, most grids are manufactured from Pb–Sb or Pb–Ca. Antimony is typically alloyed in amounts ranging from 4 to 18% Sb, and commercial Pb–Sb alloys typically include small amounts of As, Cu, and Sn [80]. Batteries manufactured using Pb–Sb alloys have self-discharge problems, and this is overcome in certain applications by the use of Pb–Ca alloys; these alloys typically contain 0.07% Ca and 1% Sn. For a detailed discussion of grid materials, the reader is referred to the review of Perkins [80].

The initial paste is manufactured by mixing PbO, sulphuric acid, water, and certain additives. The oxide is formed by air oxidation of lead dust and is normally $< 50\ \mu m$ particle size. Three groups of additives are added to the negative paste, alone or in combination, to improve performance:

(a) Inorganic additives, mainly $BaSO_4$ — typically 0.1 - 0.3 wt.%.

(b) Organic additives such as lignin or its derivatives — typically 0.1 - 0.3 wt.%.

(c) Lampblack (soot) — typically 0.1 - 0.3 wt.%.

These additives are designated as expanders [4] and their influence on battery performance will be discussed in Section 4. Lignin-type compounds are obtained from purified and dried wood flour, and a typical lignin structure, suggested by Adler [81], is shown in Fig. 1. Lignin molecules are formed from three primary precursors: *p*-coumaryl alcohol, coniferyl alcohol and sinapyl alcohol [82]; the proportions of these precursors vary with the origin of the lignin [83, 84] and may have some significance for battery performance.

When the partially oxidised lead powder is mixed with water and H_2SO_4, complex chemical reactions give rise to a paste composed of Pb,

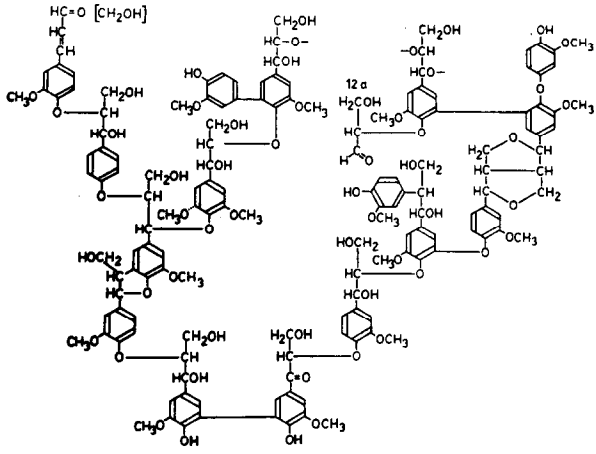

Fig. 1. Schematic formula for a section of spruce lignin, according to Adler [81].

PbO, $PbSO_4$, $PbO \cdot PbSO_4$ and $3PbO \cdot PbSO_4 \cdot H_2O$ [80, 85, 86]. The exact composition depends on factors such as starting mixture, rate of mixing, and temperature. At equilibrium, the major compounds are PbO and $3PbO \cdot PbSO_4 \cdot H_2O$ [85]. After mixing, the paste is applied to the electrode grid and cured.

(ii) Curing

The plates are generally cured over a period of days in a humid atmosphere. Three main effects are observed [85]:

(a) paste hardening;

(b) a reduction of free lead content by conversion to PbO;

(c) a corrosive attack on the metal grid, which promotes bonding of the active material.

The residual moisture content is important in determining the rate of oxidation of the remaining free lead [87], probably because of the dissolved oxygen [88]. The type and proportion of the basic sulphates occurring in the cured paste depend on the curing conditions. At temperatures and humidities around normal, a cured paste contains mainly $PbO \cdot PbSO_4$ and $3PbO \cdot PbSO_4$, but at curing temperatures > 70 °C and higher humidities, tetrabasic lead sulphate $4PbO \cdot PbSO_4$ predominates [5, 89, 90]. Schlotter and Fleischmann [91, 92] have demonstrated that the pore volume of the cured paste varies linearly with dry paste density, and the gradient of the line varies with curing conditions. It was also demonstrated that pore volumes were highest in the pastes which contained the greater amounts of tetrabasic lead sulphate; this observation is significant for the optimisation of plate capacity (see Section 4).

(iii) Forming

Commercial battery plates are usually galvanostatically formed in dilute H_2SO_4, but during the early stages of formation the interior of the plate remains alkaline, allowing more efficient reduction [85]. Earlier work demonstrated that the formation of sponge lead occurred by an electrodeposition process [6, 93], and the nature of the deposit depended on the forming conditions [94 - 96]. These observations have been confirmed in a comprehensive investigation of the formation process by Pavlov and his coworkers [86, 97]. Electron microprobe analysis, X-ray analysis, and microscopy were used to look at the formation process [86] under normal galvanostatic conditions, and two stages were observed. During the first stage, some of the PbO (free or bound to $3PbO \cdot PbSO_4 \cdot H_2O$) was reduced to Pb, while another part was transformed into $PbSO_4$. This initially formed Pb provides a network for the deposition of the lead subsequently formed in the second stage when $PbSO_4$ is reduced to Pb. During formation the pore radii and the active mass increase. The advance of these processes across the plate shows that the reaction is initiated at the grid bars [86, 93, 97, 99]. A zone consisting of Pb and $PbSO_4$ crystals is formed which advances along the plate surface, and then penetrates into the interior of the plate. The first stage ends when the paste is totally converted to Pb–$PbSO_4$, and the formation of the plate ends when the $PbSO_4$ is reduced to Pb.

3. Physical characterisation of the porous lead electrode

The morphology of the charged porous lead electrode approaches the ideal configuration for a porous lead electrode [1]. The structure of the formed electrode has been microscopically studied by a number of workers [93, 98 - 102] and lead crystals with rough porous surfaces have been observed. This structure gives a high surface area and an unimpeded circulation of electrolyte through the matrix. It also possesses good material strength and electronic conduction properties [1].

Simon and Jones [93] demonstrated that electrode morphology depended on forming conditions such as current density, temperature, and electrolyte concentration. The major influence was found to be electrolyte concentration; as the concentration increased, the surface area/porosity of the electrode decreased. The major influences on electrode structure are generally considered to be the expander additions [1, 4] (these will be considered further in Section 4). In the presence of lignin, smaller, more uniform, rough-surfaced and porous particles of lead are observed in the charged lead electrode. Therefore, the presence of lignin effects a greater surface area/porosity [101 - 106], and improved cycling capabilities [104, 107 - 110]. At high cycle numbers, the specific surface area decreases with cycle number [8] as the lead crystals agglomerate into large particles which are

difficult to discharge [106]. The number of lead nucleation centres was found to increase with cycle number over the first 10 or 15 cycles for a porous lead micro-electrode containing lignin [103]. It was concluded that the surface area/porosity of the lignin-containing electrode increased over the first few cycles. This conclusion confirmed other measurements of specific surface area [4, 8] and end-of-charge voltage [4, 101].

Values for the specific and effective surface area of the porous lead electrode have already been given in Section 1 which show an order of magnitude difference. This is probably reflected in the relatively low values of double layer capacitance of 10 - 11 μF cm^{-2}, based on B.E.T. surface [7, 111, 112]. Micka *et al.* [113] have recently investigated the structural characteristics of the positive and negative electrodes. The formed active mass of the lead electrode was found to have a mean composition of 76.8% Pb; 3.3% $PbSO_4$; and 19.9% PbO (tetragonal). The mean porosity after formation was 0.55 and this value fell linearly with the charge passed during discharge. The apparent density (including voids) on formation was 4.70 g cm^{-3}, and comparison with the density of Pb (11.34 g cm^{-3}) indicates the effect of porosity. These authors also found that the negative electrode had a more regular structure than the positive, which gave better transport properties and a correspondingly lower value for the tortuosity factor. The mean pore radius was found to be an order of magnitude greater for the negative electrode, while the specific surface area was an order of magnitude lower. After charging, the tortuosity factor may be higher owing to entrapped hydrogen bubbles in the matrix [114], but this value decreases as the bubbles are removed by capillary action. This phenomenon also affects measurements of inter-electrode solution conductivity [112].

Bode [4] examined the variation of porosity during the formation process and in subsequent cycling. A volume decrease in the solid mass of the lead electrode was observed during formation, and this was accompanied by an increase in pore volume. The author quoted a mean pore diameter of 4 - 5 μm, with a narrow pore spectrum, for the formed negative. A pore volume of 0.25 cm^3 g^{-1} was also quoted, which is in close agreement with the 0.215 cm^3 g^{-1} measured by Winsel *et al.* [36]. The specific surface area (0.5×10^4 cm^2 g^{-1}) and pore diameter of the electrode were found to remain constant during subsequent cycling, but the porosity increased from 0.69 for the formed mass to 0.80 at the 50th cycle. These physical characteristics of the porous lead electrode: surface area, pore dimensions, and porosity, govern its response in electrochemical investigations.

4. The electrochemistry of the porous lead electrode in H_2SO_4

(i) The function of expanders

In Section 2(i), the use of expanders in the active material of the porous lead electrodes was described, and their effect on morphology was described

in Section 3. The high rate, low temperature performance of the lead–acid battery is limited by the negative electrode [1] (see below), and this is improved by expander additions [104, 106, 107, 115]. Many effects have been ascribed to lignin and its derivatives. These compounds have been found to adsorb on the surface of metallic lead [106, 116 - 118], and Simon [119] suggested that lignins had to be first oxidised in solution before adsorption could take place. Many authors have suggested that lignins beneficially affect the lead structure formed on charge, and, hence, the surface area [101 - 106, 120], presumably because lignin adsorption lowers the surface energy of the lead, making the formation of smaller and more loosely packed lead crystals more favourable [4]. Lignins are also claimed to influence the formation of $PbSO_4$, making the crystals smaller, the film more porous, and easier to reduce [104, 107, 121 - 123]. The onset of passivation is also said to be delayed by lignins [106, 118, 124], while Le Mehaute observed the effect of lignins before and after passivation [125]. Recent work in this laboratory has demonstrated that lignin has no direct electrochemical effect on the discharge process [103], but the larger surface area probably makes the more widely dispersed $PbSO_4$ film thinner and easier to reduce. Lignin also improves the cycling behaviour of the electrode by reducing the rate and extent of capacity loss [101, 106]. Mahato [106] also investigated the influence of different lignosulphonate salt cations on the charge and discharge processes and found that the sodium salt gave the best performance.

The function of the other two expander additions in the negative electrode is more easily defined. Lampblack has no electrochemical effect on battery performance and is added to increase electrode conductivity during formation. $BaSO_4$ acts synergistically with lignin to give an even greater effective surface area/porosity, and, hence, capacity [101, 105, 107]. This is because $BaSO_4$ provides nucleation centres for $PbSO_4$, with which it is isomorphous [101, 103, 107]. Hence, $BaSO_4$ influences the size of $PbSO_4$ crystals [108], and probably makes discharge more efficient, and the resultant $PbSO_4$ film easier to reduce. The formation of $PbSO_4$ from Pb — the oxidation or discharge process, is the critical capacity-determining process at the porous lead electrode.

(ii) The discharge of the porous lead electrode

In the battery industry, the performance of the lead electrode is generally assessed galvanostatically. The electrode is discharged at constant-current, and the resultant potential–time behaviour of the electrode is recorded. Features of this E–t plot include: (a) resistance of solution and materials, (b) double layer capacity, (c) supersaturation, nucleation, and crystallisation phenomena, (d) the discharge of Pb to $PbSO_4$, and (e) rapid polarisation owing to acid depletion and pore plugging [2]. The performance (capacity) of the electrode is assessed by the time taken, t_d, to reach phase (e) at different discharge currents.

The performance characteristics of the lead–acid battery are complex and numerous, and battery developers have been content to assess perfor-

mance in terms of empirical relationships such as the Peukert equation [126]

$$I^x t_d = K \tag{8}$$

where x and K are constants determined from discharge data. For intermediate currents, $x \approx 1.3 - 1.4$, but tends to 2 at high current and 1 at low current, and the equation is therefore only valid at intermediate currents [4].

Equation (8) simply expresses experimental observations that capacity decreases with increasing load (discharge rate) [127 - 131]; where discharge is limited by the formation of $PbSO_4$ and concentration changes at the electrode surface [9, 100, 131]. $PbSO_4$ crystal size is found to decrease with increasing discharge rate [100, 128, 132], and this makes the passivation of the lead active surface more effective.

A number of workers have suggested that the discharge (and charge) processes at the negative electrode involve a dissolution–precipitation mechanism [2, 37, 127, 133]. The discharge and charge of lead electrodes may then be considered as anodic dissolution, and cathodic deposition, of a soluble lead species. S.e.m. evidence has been used to support this hypothesis [134, 135], and a soluble lead species has been detected using a flat lead electrode at small overpotentials [136 - 142].

As the temperature is decreased below 0 °C, the capacity of the porous lead electrode decreases [127, 143], as does the size of the $PbSO_4$ crystals formed [132]. Berndt [127] showed that at 40 °C, ~35 - 60% of the theoretical capacity could be discharged, depending on discharge rate, but at −30 °C this fell ~10 - 30%. The author also observed variations in the constants, x and K, of the Peukert equation (8). As the temperature decreased, x increased and K decreased, and the author concluded that these constants reflected the complex nature of the interactions involved. Winsel *et al.* [36] examined the high rate discharge of the porous lead electrode at −18 °C and found that the capacity varied linearly with the square of the surface area. Mahato [106] observed a linear relationship between capacity and surface area under similar conditions, but the results showed a lot of scatter. Winsel *et al.* [36] predicted, and observed "ice passivation" of the porous lead electrode at −18 °C. In this laboratory, the capacity behaviour of the flat lead electrode at ~22 °C and −30 °C was found to be similar [128, 130, 144]. At ~22 °C, discharge rate had little effect on the observed capacity of a porous microelectrode [128, 130]. However, a significant effect was observed at −30 °C [143], and it was concluded that high rate discharge capacity limitation at −30 °C involved "ice passivation" of the porous lead electrode [143].

The potentiostatic technique has been little used for the study of the porous lead electrode. In this laboratory, we have confirmed the prediction of eqn. (7) that the response of a porous lead electrode to double-layer charging is a current which decays as $1/\sqrt{t}$ [130]. The predictions of eqn. (3) were also confirmed. At short times, the transient response of a solid lead electrode to a potential oxidation step was a current that rose

linearly with time. On the porous electrode, the current rose as the square-root of time [130]. It was concluded that the nucleation and growth of $PbSO_4$ at solid and porous lead electrodes followed an instantaneous nucleation and two-dimensional growth process, controlled by crystallisation processes. It was also demonstrated that two competing processes occur on discharge to limit the capacity of the electrode. At low discharge rates the conversion of all available Pb to $PbSO_4$ predominates, but at high discharge rates the effect of pore plugging by $PbSO_4$ becomes more significant [130]. At −30 °C and high discharge rates "ice passivation" also becomes a significant capacity-limiting process [143].

The introduction of mark/space motor controllers in electric vehicles has necessitated the investigation of the lead–acid battery under pulsed current discharge. Jayne [145] has investigated the behaviour of lead–acid cells under continuous discharge, interrupted discharge, and pulsed discharge conditions. The constant current discharge behaviour of the cell was found to provide a conservative estimate of the available capacity from pulsed and interrupted discharge, provided a mean value of discharge current was used. The improvement in performance was attributed to a recovery phenomenon which occurs during current interruption. Turner [146] explained this phenomenon in terms of the relaxation of concentration depletion. Alternatively, the pulse time durations are so short compared with the total discharge time, that the average current and electrolyte depletions will look the same as in the continuous case. Berndt's work on the porous lead electrode [127] confirms these observations somewhat, where electrodes fully discharged at various rates and temperatures could be further discharged at 25 °C.

(iii) The charge of the porous lead electrode

Data on the reduction (charge) of the porous lead electrode are scarce. Peters *et al.* [147] showed that the high-rate charging efficiency of 91% at 40 °C was reduced to 70% at 0 °C. Willihnganz [132] observed that porous lead electrodes tested at −40 °C accepted charge at a rate proportional to the degree of previous discharge. Bode [4] found that the charge rate was significantly reduced below 0 °C, and, at −50 °C, charging became impossible. Willihnganz [132] observed that the charge rate increased as the size of the $PbSO_4$ crystals formed on discharge decreased, and crystal size decreased with decreasing discharge temperature and increasing discharge rate.

The reduction of sulphated solid lead electrodes has been studied in this laboratory in order to examine the effect of organics on the electrocrystallisation of Pb from $PbSO_4$ [148]. It was concluded that the process conformed to an instantaneous nucleation and two-dimensional growth process at a flat electrode. More recent work showed that sulphated (solid and porous) electrodes behaved as true porous electrodes on reduction (see eqn. (3)). The current in the transient resulting from a potential reduction step rose as the square root of time [149], in a similar manner to the oxidation of the porous lead electrode [130]. Reduction of $PbSO_4$ to Pb, therefore, proceeds

by an instantaneous nucleation and two-dimensional growth process, but both solid and porous electrodes behave as porous electrodes. The current decay rate in the reduction transient was found to vary with the degree of prior galvanostatic discharge [149], and the expander additions to the active material [103]. It was concluded that the decay rate reflected the surface area/porosity of the electrode.

The reduction of the sulphated solid electrodes at −30 °C did not show the same behaviour as the porous electrode. On the solid electrode, only a falling transient, indicative of a diffusion-limited process, was observed [144]. The current response of a porous lead electrode to a potential-reduction step at −30 °C, was a rising and falling transient [143]. This transient was obscured by the hydrogen evolution reaction, because the overpotential for lead formation at the porous lead electrode was greater at −30 °C than at ~22 °C.

Acknowledgement

This review was prepared during a tenancy of a Lucas Research Scholarship (by J.B.L.) at Loughborough University.

List of symbols

C	concentration at pore mouth
C'	capacitance
D	diffusion coefficient
E	potential
F	Faraday constant
i	current entering pore
i_0	exchange current density
I	discharge current (galvanostatic)
K	constant in Peukert equation
l	pore length
n	number of electrons transferred
r	pore radius
R	gas constant
Z'	charge transfer resistance
t	time
t_d	time to galvanostatic discharge
T	temperature
x	constant in Peukert equation
Z	solution (or electrode) resistance
α	transfer coefficient
κ	solution conductivity
η	overpotential
θ	porosity

References

1 J. Burbank, A. C. Simon and E. Willihnganz, in P. Delahay (ed.), *Adv. Electrochem. Electrochem. Eng., 8* (1971) 157.
2 P. Ruetschi, *J. Power Sources, 2* (1977/78) 3.
3 D. A. J. Rand, *J. Power Sources, 4* (1979) 101.
4 H. Bode, *Lead–Acid Batteries*, Wiley-Interscience, New York, 1977.
5 G. W. Vinal, *Storage Batteries*, Wiley, New York, 4th Edn., 1955.
6 T. I. Popova and B. N. Kabanov, *Zh. Prikl. Khim., 32* (1959) 326.
7 R. F. Amlie, J. B. Ockerman and P. Ruetschi, *J. Electrochem. Soc., 108* (1961) 377.
8 M. R. Skalozubov, *Zh. Prikl. Khim., 35* (1962) 1812.
9 E. Willihnganz, *J. Electrochem. Soc., 102* (1955) 99.
10 D. Simonsson, *Thesis*, Inst. Kemist. teknologi, Kungl, Tekniska Högskolan, Stockholm, 1973,
11 V. S. Daniel'-Bek, *Zh. Fiz. Khim., 22* (1948) 697.
12 R. de Levie, in P. Delahay (ed.), *Adv. Electrochem. Electrochem. Eng., 6* (1967) 329.
13 J. O'M. Bockris and S. Srinivasan, *Fuel Cells: Their Electrochemistry*, Ch. V, McGraw-Hill, New York, 1969.
14 E. A. Grens, *Electrochim. Acta, 15* (1970) 1047.
15 J. Newman and W. Tiedmann, *Am. Inst. Chem. Eng. J., 21* (1975) 25.
16 A. Winsel, *Z. Elektrochem., 66* (1962) 287.
17 J. Euler and W. Nonnenmacher, *Electrochim. Acta, 2* (1960) 268.
18 J. Euler, *Electrochim. Acta, 8* (1963) 409.
19 J. S. Newman and C. W. Tobias, *J. Electrochem. Soc., 109* (1962) 1183.
20 L. G. Austin, *Trans. Faraday Soc., 60* (1964) 1319.
21 O. S. Ksenzhek and V. V. Stender, *Dokl. Akad. Nauk SSSR, 107* (1956) 280.
22 O. S. Ksenzhek and V. V. Stender, *Dokl. Akad. Nauk SSSR, 106* (1956) 487.
23 O. S. Ksenzhek and V. V. Stender, *Zh. Fiz. Khim., 31* (1957) 117.
24 R. de Levie, *Electrochim. Acta, 8* (1963) 751.
25 F. A. Posey and T. Morozumi, *J. Electrochem. Soc., 113* (1966) 176.
26 O. S. Ksenzhek, *Zh. Fiz. Khim., 36* (1960) 243.
27 O. S. Ksenzhek, *Zh. Fiz. Khim., 37* (1963) 2007.
28 O. S. Ksenzhek, *Zh. Fiz. Khim., 38* (1964) 1846.
29 I. G. Guruvich and V. S. Bagotskii, *Electrochim. Acta, 9* (1964) 1151.
30 I. G. Guruvich and V. S. Bagotskii, *Electrokhimiya, 1* (1965) 1102.
31 E. A. Grens and C. W. Tobias, *Ber. Bunsenges. Phys. Chem., 68* (1964) 236.
32 S. K. Rangarajan, *J. Electroanal. Chem., 22* (1969) 89.
33 K. Kunimatsu, *J. Res. Inst. Catal. Hokkaido Univ., 20* (1972) 1.
34 J. S. Dunning and D. N. Bennion, *J. Electrochem. Soc., 120* (1973) 906.
35 S. Szpak, A. Nedoluha and T. Katan, *J. Electrochem. Soc., 122* (1975) 1054.
36 A. Winsel, U. Hullmeine and E. Voss, *J. Power Sources, 2* (1978) 369.
37 K. J. Vetter, *Chem. Ing. Tech., 45* (1973) 213.
38 R. C. Alkire, E. A. Grens and C. W. Tobias, *J. Electrochem. Soc., 116* (1969) 1328.
39 R. C. Alkire and B. Place, *J. Electrochem. Soc., 119* (1972) 1678.
40 J. S. Dunning, D. N. Bennion and J. Newman, *J. Electrochem. Soc., 118* (1971) 1251.
41 J. S. Dunning and D. N. Bennion, *Proc. Advances in Battery Technology Symp.*, The Electrochemical Society, Inc., Southern California — Nevada Section, Vol. 5, 1969.
42 H. Gu, D. N. Bennion and J. Newman, *J. Electrochem. Soc., 123* (1976) 1364.
43 D. Gidaspow and B. S. Baker, *J. Electrochem. Soc., 120* (1973) 1005.
44 K. Micka and I. Rousar, *Electrochim. Acta, 19* (1974) 499.
45 K. Micka and I. Rousar, *Electrochim. Acta, 18* (1973) 629.
46 K. Micka and I. Rousar, *Electrochim. Acta, 21* (1976) 599.
47 D. Simonsson, *J. Electrochem. Soc., 120* (1973) 151.
48 D. Simonsson, *J. Appl. Electrochem., 3* (1973) 261.

49 D. Simonsson, *J. Appl. Electrochem., 4* (1974) 109.
50 M. Risberg, P. Sahleström and D. Simonsson, *Rep. TRITHA-KTE-1003*, Royal Inst. Technol., Stockholm, 1973.
51 H. Lehning, *Elektrotech. Z., 93A* (1972) 62.
52 W. Runge, *Elektrotech. Z., 93A* (1972) 67.
53 A. D. Turner, *A.E.R.E. Rep. No. R8931*, 1978.
54 W. Stein, *Naturwissenschaften, 45* (1958) 459.
55 W. Stein, *Thesis*, Techn. Hochschule Aachen, 1959.
56 R. J. Brodd, *Electrochim. Acta, 11* (1966) 1107.
57 F. G. Will and H. J. Hess, *J. Electrochem. Soc., 120* (1973) 1.
58 S. Szpak, J. D. Elwin and T. Katan, *Electrochim. Acta, 11* (1966) 934.
59 S. Szpak and T. Katan, *J. Electrochem. Soc., 122* (1975) 1063.
60 T. Katan, J. Savory and J. Perkins, *J. Electrochem. Soc., 126* (1979) 1835.
61 V. Panov, V. S. Borokov and P. D. Lukovtsev, *Elektrokhimiya, 5* (1969) 180.
62 E. G. Gagnon and L. G. Austin, *J. Electrochem. Soc., 118* (1971) 497.
63 P. Bro and H. Y. Kang, *J. Electrochem. Soc., 118* (1971) 519.
64 Z. Nagy and J.O'M. Bockris, *J. Electrochem. Soc., 109* (1972) 1129.
65 T. Katan, S. Szpak and D. N. Bennion, *J. Electrochem. Soc., 120* (1973) 883.
66 T. Katan, S. Szpak and D. N. Bennion, *J. Electrochem. Soc., 121* (1974) 757.
67 T. Katan, H. Gu and D. N. Bennion, *J. Electrochem. Soc., 123* (1976) 1370.
68 S. Tudor, A. Weisstuch and S. H. Davang, *Electrochem. Tech., 3* (1965) 90.
69 S. Tudor, A. Weisstuch and S. H. Davang, *Electrochem. Tech., 4* (1966) 406.
70 H. Bode and J. Euler, *Electrochim. Acta, 11* (1966) 1211.
71 H. Bode and J. Euler, *Electrochim. Acta, 12* (1967) 84.
72 H. Bode, E. Rieder and H. Schmitt, *Electrochim. Acta, 11* (1966) 1231.
73 H. Liebssle, H. Reber, W. Herrmann and E. Zehender, *Bosch. tech. Ber., 2* (1968) 159.
74 H. Bode, H. Panesar and E. Voss, *Naturwissenschaften, 55* (1968) 541.
75 H. Bode, H. Panesar and E. Voss, *Chem.-Ing. Tech., 41* (1969) 878.
76 H. Haebler, H. Panesar and E. Voss, *Electrochim. Acta, 15* (1970) 1421.
77 W. S. Yantschenko and I. A. Selitsky, *Elektrotekhnika, 37* (1966) 34.
78 C. Liebnow, *Z. Elektrochem., 4* (1897) 61.
78a A. Winsel, *Ber. Busenges Phys. Chem., 79* (1975) 828.
79 C. Fauré, *French patent 141,057 (1881).*
80 J. Perkins, *Mater. Sci. Eng., 28* (1977) 167.
81 E. Adler, *Sven. Kem. Tidskr., 80* (1968) 279.
82 K.-E. Eriksson and U. Lindholm, *Sven. Papperstidn., 74* (1971) 701.
83 T. K. Kirk, *Annu. Rev. Phytopathol., 9* (1971) 185.
84 K. V. Sarkanen and C. H. Ludwig, in K. V. Sarkanen and C. H. Ludwig (eds.), *Lignins: Occurrence, Formation, Structure and Reactions*, Wiley-Interscience, New York, 1971, p. 1.
85 S. C. Barnes and R. T. Mathieson, in D. H. Collins (ed.), *Batteries 2*, Pergamon, London, 1965, p. 41.
86 D. Pavlov, V. Iliev, G. Papazov and E. Bashtavelova, *J. Electrochem. Soc., 121* (1974) 854.
87 R. H. Greenburg, F. B. Finnan and B. J. Agruss, *J. Electrochem. Soc., 98* (1951) 474.
88 F. C. Will, *J. Electrochem. Soc., 110* (1963) 145.
89 J. Armstrong, I. Dugdale and W. J. McCusker, in D. H. Collins (ed.), *Power Sources, 1966*, Pergamon, London, 1967, p. 163.
90 A. C. Simon, in D. H. Collins (ed.), *Batteries 2*, Pergamon, London, 1965, p. 63.
91 C. W. Fleischmann and W. J. Schlotter, *J. Electrochem. Soc., 123* (1976) 969.
92 W. J. Schlotter and C. W. Fleischmann, *J. Electrochem. Soc., 124* (1977) 1487.
93 A. C. Simon and E. L. Jones, *J. Electrochem. Soc., 109* (1962) 760.
94 S. C. Barnes, *Electrochim. Acta, 5* (1961) 79.
95 S. C. Barnes and G. G. Storey, *J. Inst. Met., 90* (1961/62) 336.
96 A. K. Graham and H. L. Pinkerton, *Trans. Inst. Met. Finish., 40* (1963) 249.
97 D. Pavlov, *J. Electroanal. Chem., 72* (1976) 319.

98 A. C. Simon, in D. H. Collins (ed.), *Power Sources 2*, Pergamon, London, 1970, p. 33.
99 N. E. Bagshaw and K. P. Wilson, *Electrochim. Acta, 10* (1965) 867.
100 E. Willihnganz, *Trans. Electrochem. Soc., 79* (1941) 243.
101 N. A. Hampson, J. B. Lakeman, J. G. Smith and K. S. Sodhi, *Surf. Technol.*, in press.
102 J. R. Pierson, P. Gurlusky, A. C. Simon and S. M. Caulder, *J. Electrochem. Soc., 117* (1970) 1463.
103 N. A. Hampson and J. B. Lakeman, *J. Electroanal. Chem.*, in press.
104 A. C. Simon, S. M. Caulder, P. J. Gurlusky and J. R. Pierson, *J. Electrochem. Soc., 121* (1974) 463.
105 A. C. Simon, S. M. Caulder, P. J. Gurlusky and J. R. Pierson, *Electrochim. Acta, 19* (1974) 739.
106 B. K. Mahato, *J. Electrochem. Soc., 124* (1977) 1663.
107 E. Willihnganz, *Trans. Electrochem. Soc., 92* (1947) 281.
108 A. C. Zachlin, *J. Electrochem. Soc., 98* (1951) 325.
109 E. J. Ritchie, *Trans. Electrochem. Soc., 92* (1947) 229.
110 E. J. Ritchie, *J. Electrochem. Soc., 100* (1953) 53.
111 P. Ruetschi, J. B. Ockerman and R. Amlie, *J. Electrochem. Soc., 107* (1960) 325.
112 W. Tiedmann and J. Newman, *J. Electrochem. Soc., 122* (1975) 70.
113 K. Micka, M. Svatá and V. Koudelka, *J. Power Sources, 4* (1979) 43.
114 I. L. Romanova and I. A. Selitskii, *Elektrokhimiya, 6* (1970) 1776.
115 A. P. Hauel, *Trans. Electrochem. Soc., 78* (1940) 231.
116 T. F. Sharpe, *Electrochim. Acta, 14* (1969) 635.
117 T. F. Sharpe, *J. Electrochem. Soc., 116* (1969) 1639.
118 G. Archdale and J. A. Harrison, *J. Electroanal. Chem., 47* (1973) 93.
119 W. Simon, *Bosch. Tech. Ber., 1* (1966) 234.
120 T. J. Hughel and R. H. Hammer, in D. H. Collins (ed.), *Power Sources 3*, Oriel Press, Newcastle upon Tyne, 1971, p. 35.
121 Y. B. Kasparov, E. G. Yampol'skaya and B. N. Kabanov, *Zh. Prikl. Khim., 37* (1964) 1936.
122 E. G. Yampol'skaya, M. I. Ershova, I. I. Astakhov and B. N. Kabanov, *Elektrokhimiya, 2* (1966) 1327.
123 E. G. Yampol'skaya, M. I. Ershova, V. V. Surikov, I. I. Astakov and B. N. Kabanov, *Elektrokhimiya, 8* (1972) 1236.
124 M. P. J. Brennan and N. A. Hampson, *J. Electroanal. Chem., 48* (1973) 465.
125 A. Le Mehaute, *J. Appl. Electrochem., 6* (1976) 543.
126 W. Peukert, *Elektrotech. Z., 18* (1897) 287.
127 D. Berndt, in D. H. Collins (ed.), *Power Sources 2*, Pergamon, London, 1970, p. 17.
128 N. A. Hampson and J. B. Lakeman, *Surf. Technol., 9* (1979) 97.
129 N. A. Hampson and J. B. Lakeman, *J. Appl. Electrochem., 9* (1979) 403.
130 N. A. Hampson and J. B. Lakeman, *J. Electroanal. Chem., 107* (1980) 177.
131 M. I. Gillibrand and G. R. Lomax, *Electrochim. Acta, 8* (1963) 693.
132 E. Willihnganz, in D. H. Collins (ed.), *Power Sources 5*, Academic Press, London, 1975, p. 43.
133 S. Hisano, *Kogyo Kagaku Kasshi, 62* (1959) 378.
134 J. L. Weininger, *J. Electrochem. Soc., 121* (1974) 1454.
135 J. L. Weininger and F. W. Secor, *J. Electrochem. Soc., 121* (1974) 1541.
136 G. Archdale and J. A. Harrison, *J. Electroanal. Chem., 34* (1972) 21.
137 G. Archdale and J. A. Harrison, *J. Electroanal. Chem., 39* (1972) 357.
138 G. Archdale and J. A. Harrison, *J. Electroanal. Chem., 43* (1973) 321.
139 A. N. Fleming, J. A. Harrison and J. Thompson, in D. H. Collins (ed.), *Power Sources 5*, Academic Press, London, 1975, p. 1.
140 A. N. Fleming and J. A. Harrison, *Electrochim. Acta, 21* (1976) 905.
141 R. D. Armstrong and K. L. Bladen, *J. Appl. Electrochem., 7* (1977) 345.
142 N. A. Hampson and J. B. Lakeman, *J. Power Sources, 4* (1979) 21.

143 N. A. Hampson and J. B. Lakeman, *J. Appl. Electrochem.*, in press.
144 N. A. Hampson and J. B. Lakeman, *J. Electroanal. Chem.*, *108* (1980) 347.
145 M. G. Jayne, in D. H. Collins (ed.), *Power Sources 6*, Academic Press, London, 1977, p. 35.
146 A. D. Turner, *A.E.R.E. Rep. No. R8932*, 1978.
147 K. Peters, A. I. Harrison and W. H. Durant, in D. H. Collins (ed.), *Power Sources 2*, Pergamon, London, 1970, p. 1.
148 M. P. J. Brennan and N. A. Hampson, *J. Electroanal. Chem.*, *52* (1974) 1.
149 N. A. Hampson and J. B. Lakeman, *J. Electroanal. Chem.*, in press.